Magnetoelastic excitation of single nanomagnets for optical measurement of intrinsic Gilbert damping

W. G. Yang, M. Jaris, D. L. Hibbard-Lubow, C. Berk, and H. Schmidt

Phys. Rev. B **97**, 224410 — Published 12 June 2018

DOI: 10.1103/PhysRevB.97.224410

Magnetoelastic Excitation of Single Nanomagnets for Optical Measurement of Intrinsic Gilbert Damping

W.G. Yang [*], M. Jaris [*], D. L. Hibbard-Lubow, C. Berk, and H. Schmidt [†]

School of Engineering, University of California Santa Cruz, 1156 High Street, Santa Cruz, California 95064, USA

We report a novel all-optical technique to drive and probe the spin dynamics of single nanomagnets. Optically generated surface acoustic waves (SAWs) drive the magnetization precession in nanomagnets via magneto-elastic (MEL) coupling. We investigate the field-swept dynamics of isolated Ni nanomagnets at various SAW frequencies, and show that this method can be used to accurately determine the intrinsic Gilbert damping of nanostructured magnetic materials. This technique opens a new avenue for studying the spin dynamics of nanoscale devices using non-thermal ("cold") excitation, enabling direct observation of the MEL driven dynamics.

[*] These authors contributed equally to this work
[†] To whom correspondence should be addressed. Electronic mail: hschmidt@soe.ucsc.edu

Nanostructured magnetic devices have been identified as leading candidates for next generation data storage, quantum computation, low power magnetic logic [1] and neuromorphic computing [2]. The operation characteristics of these technologies are closely related to their dynamic magnetic properties, such as the Gilbert damping parameter (α) which directly determines the switching power threshold and operating speed of spin-transfer torque memory [3]. Thus, the direct measurement of a single nanomagnet is crucial to the development of spintronic devices, but many conventional techniques do not possess the sensitivity to resolve the small-angle magnetization precession of isolated nanostructures. One approach to overcome this problem is to measure an array of nanomagnetic devices. This, however, yields an ensemble signal that is heavily influenced by the magnetostatic interactions of neighboring elements and dynamic dephasing between elements, both of which mask the intrinsic spin dynamics [4–6]. Instead, a variety of novel measurement techniques have been developed to probe the dynamic behavior of magnetic nanostructures [7–15], but only a few of these approaches such as cavity-enhanced magneto-optic Kerr effect (CE-MOKE) [16], spin-torque ferromagnetic resonance (ST-FMR) [17] and heterodyne magneto-optical microwave microscopy [18] (H-MOMM) have been used to accurately determine the damping parameter. Here, we introduce a new technique to excite and probe the magnetization dynamics of a single nanomagnet. Surface acoustic waves (SAWs) are optically generated on a one-dimensional nanowire array and used to excite narrow-band magnetization precessions in a single, remote nanomagnet via magneto-elastic (MEL) coupling (Fig. 1(a)). These non-thermal ("cold") excitations can be measured with time-resolved MOKE spectroscopy and are qualitatively different from all-optical TR-MOKE dynamics. Specifically, we use this approach to measure the intrinsic Gilbert damping in single Ni nanomagnets and show that α can be extracted directly from the range of applied fields over which the magnetic precession is excited by the SAW. This demonstrates that the larger effective damping α_{eff} observed in optically excited single nanomagnets is due to thermal effects.

Previous studies have used SAWs to excite and detect the magnetization dynamics of films [19–21] and nanomagnet arrays [22–24], and found that a magneto-elastic resonance occurs which pins magnetic response to the SAW frequency (f_{SAW}) over a range of applied fields. Thus, magneto-elastic coupling has been established as an alternative means to study the dynamic properties of magnetic.

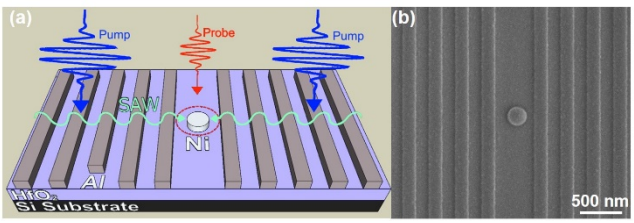

FIG. 1 (color online). (a) Schematic plot of all-optical "cold" magnetization excitation in single Ni nanomagnet (b) SEM image of a Ni nanomagnet embedded between an Al nanowire array (pitch = 300 nm).

In order to investigate the SAW driven magnetization dynamics of a single nanomagnet, a nickel (Ni) nanocylinder (200 nm diameter, 30 nm thick) was defined between two sets of identical, non-magnetic aluminum (Al) bars (Fig. 1(b)) on a (100) Si substrate capped by a 110 nm thick hafnium oxide antireflection (AR) coating [25–27] utilizing multilevel electron beam lithography (EBL), electron beam evaporation, and lift-off processes. Four sets of Al bars ($width = 100$, $thickness = 30nm$) were fabricated, each with a different pitch ($p = 250$, 300, 350, and 400 nm), corresponding to a distinct SAW frequency (f_{SAW} = 11.45, 9.75, 8.65, and 7.75 GHz) that is determined by the relation: $f_{SAW} = v_s / p$ [22], where v_s is the speed of sound along the sample surface. To excite SAWs, the Al bars are illuminated by an ultrafast pump pulse (modulated at 1 kHz) which causes impulsive thermal expansion of the elements that produces a periodic elastic strain along the surface, launching SAWs that propagate at a velocity $v_s \sim 3$ km/s to the Ni nanomagnet. This method of SAW excitation has distinct advantages over other approaches, such as phononic Bragg mirrors [20] and interdigitated transducers (IDTs) [21,28]. The former requires complex deposition techniques (e.g. molecular beam epitaxy) to grow super-lattice structures, and has yet to be demonstrated in conjunction with nanopatterned structures. On the other hand, IDTs require the use of expensive piezoelectric materials that simultaneously generate acoustic and electromagnetic waves when an RF voltage is applied, which complicates the ensuing magnetization dynamics [21]. In addition, these approaches may prohibit the use of an anti-reflection surface, which is known to enhance the magneto-optic sensitivity [27]. Here, two counter-propagating strain waves are generated by identical pump pulses and consequently form a standing wave at the nanomagnet. We use two sets of bars in order to maximize the SAW strain amplitude [29], and thus the magneto-elastic field (H_{MEL}), while avoiding ablation of the aluminum bars. The pump is generated by second harmonic generation of an ultrafast Ti:Sapphire laser, and is subsequently split into two pulses using a beam splitter. Both beams are then focused onto different positions of the sample surface using a microscope objective (M = 100X, N.A. = 0.9, $\lambda =$ 400 nm, pulse width = 150 fs, FWHM ~ 3.5 μm each). The center of each pulse is at least 3 μm away from the nanomagnet to ensure there is negligible photoexcitation of the spin system. The magnetization dynamics were studied using the time-resolved magneto-optic Kerr effect (TR-MOKE) technique. A mechanically delayed probe pulse [22–24,30,31] ($\lambda =$ 800 nm, pulse width = 150 fs, FWHM ~ 0.58 μm) is focused onto the nanomagnet and experiences a gyrotropic polarization rotation upon reflection. Lock-in detection at the pump modulation frequency is used to record the Kerr rotation (magnetic) as well as the elastic motion (nonmagnetic) using the difference and sum signal of a balanced photodetector setup [32].

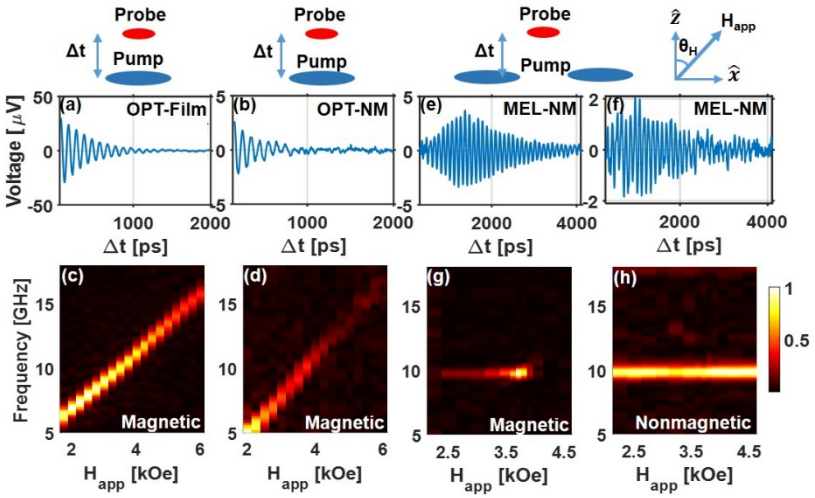

FIG. 2 (color online). TR-MOKE time traces of the optically (OPT) excited (a) Ni film and (b) isolated nanomagnet (NM), and (c,d) the corresponding field-dependent Fourier spectra of the film and NM, respectively, measured with a fixed field angle $\theta_H = 30^o$. (e) TR-MOKE trace of the MEL driven nanomagnet ($H_{app} = 3.7kOe$), and (f) nonmagnetic signal of the acoustically modulated nanostructure. The illustrations above Figs. 2(a,b) and 2(e,f) indicate the pump-probe configurations used and the applied field geometry, respectively. The field-dependent Fourier spectra of the acoustically driven NM shown in (g) which reveals strong MEL enhancement when the magnetic and nonmagnetic modes are degenerate. SAWs are identified by monitoring the transient reflectivity, shown in (h), and therefore do not depend on the applied field.

We first discuss the optically excited magnetization dynamics of an unpatterned Ni film and an isolated nanomagnet (no Al bars) measured using a standard TR-MOKE setup with overlapped pump and probe pulses. The pump quasi-instantaneously demagnetizes the sample, and within picoseconds the magnetization is restored and subsequently follows a helical trajectory back to the equilibrium orientation (Figs. 2(a) and 2(b)) [33–35]. The signal is transformed into the frequency domain by applying a Hamming window function and taking the discrete Fourier transform (DFT) of the time-evolution. The response is the well-known field-dependent Kittel mode (Figs. 2(c) and 2(d)).

Now, we turn to our new approach of triggering spin dynamics in the single nanomagnet using a magneto-elastic driving force ("cold" excitation) which yields dramatically different results. We plot the MEL driven dynamics in Fig. 2(e) ($f_{mag} = f_{SAW}$) and observe an increase in the precession amplitude between $0 < \Delta t < 1.5$ ns. To better understand this behavior, we simultaneously monitor the transient reflectivity signal (Fig. 2(f)) which reveals that the amplitude of the nonmagnetic oscillation is largest around a pump-probe delay of $\Delta t \sim 1$ ns, after which the oscillation decays with a characteristic lifetime of 1.7 ns. The delayed response matches the time it takes the strain wave to travel from the center of the

pump ($\sim 3\mu m$) at the speed of sound ($v_s \sim 3 km/s$) to the nanomagnet. It is worth noting that the MEL driven oscillation slightly lags the strain, which is consistent with the observations presented in ref. [19]. Furthermore, the magnetic precession persists almost four times longer than the dynamics instigated by ultrafast demagnetization, indicating highly efficient coupling and qualitatively different magnetization dynamics. In Figs. 2(g) and 2(h) we plot the field-dependent, SAW driven spin and elastic (nonmagnetic) Fourier spectra of the Ni nanomagnet placed between the Al bars. The oscillatory strain in the nanomagnet generates a magneto-elastic field at the acoustic frequency, resulting in a peak Fourier amplitude when the two systems are on resonance. Any field dependence of the magnetic precession frequency has been completely removed, as can be seen in Fig. 2 (g). To estimate the MEL field in the nanomagnet, we followed the multi-step simulation procedure outlined in ref [36] and estimate a peak H_{MEL} field on the order of 100 Oe.

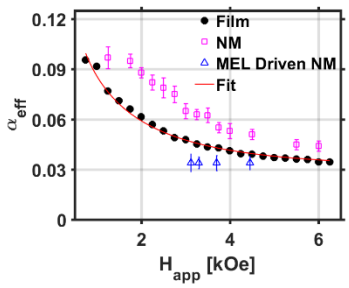

FIG. 3 (color online). Field dependence of the effective damping of the Ni film and single nanomagnet (NM) measured using conventional TR-MOKE (closed black circles and open pink squares, respectively). For comparison, the damping measured using the MEL approach is included (blue triangles). The effective damping of the film was fit using Eq. (1) to estimate the intrinsic damping (0.03) (red line), and the dashed red line is a guide to the eye.

Cold excitation does not only provide a different method to drive the magnetization precession, it also allows for a different analysis of magnetic material properties. To illustrate this, we consider the damping behavior of the optically excited spin dynamics. The magnetic precession at each field is fit using a damped harmonic function: $\sin(2\pi f_{mag}\Delta t + \phi)e^{-t/\tau_{eff}}$, where f_{mag} is the Kittel frequency and τ_{eff} is the effective lifetime of the magnetic oscillation. The frequency and lifetime directly determine the effective damping via the relation: $\alpha_{eff} = (2\pi f_{mag}\tau_{eff})^{-1}$. For the film and nanomagnet measured using the conventional TR-MOKE setup, τ_{eff} is determined by as follows: $1/\tau_{eff} = 1/\tau_{Gilb} + 1/\tau_{ext}$, where τ_{Gilb} is the lifetime determined by the intrinsic Gilbert damping (α) in the LLG equation, and τ_{ext} represents extrinsic damping mechanisms that inevitably reduce τ_{eff} and typically depend on H_{app}. In the case of an obliquely magnetized isotropic thin film, such as the unpatterned Ni, scattering between the uniform

precession and degenerate spin waves, known as two-magnon scattering (TMS), is a dominant source of extrinsic damping [37]. Therefore, to accurately estimate α from measurements of thermally excited spin dynamics, TMS contribution to the damping must be extracted from the field dependence of α_{eff} [38]. Using the model presented in ref. [39], the effective damping can be expressed as [39–42]:

$$\alpha_{eff} = \frac{1}{2\pi f_{mag}}\left[\frac{1}{\tau_{Gilb}} + \frac{1}{\tau_{TMS}}\right] \approx \frac{1}{2\pi f_{mag}}\left[\frac{\alpha\gamma(H_1+H_2)}{2} + N_0\sum_k \frac{C(k)}{2\pi f_{mag}}\mathrm{Im}\{(4\pi^2({f_{mag,k}}^2 - {f_{mag}}^2 + i\delta f_{mag,k} f_{mag})^{-1}\}\right] \quad (1)$$

where $H_{1,2}$ are effective fields that include contributions from the external field and demagnetizing field, N_0, $C(\boldsymbol{k})$, $f_{mag,k}$, and $\delta f_{mag,k}$ are the scattering intensity, correlation function, spin wave frequency, and wave-vector-dependent inverse lifetime. The scattering intensity and correlation function are determined via the following:

$$N_0 = \frac{\gamma^4}{3}(H_1+H_2)\left\langle h'^2 \right\rangle \quad (1a)$$

$$C(k) = \frac{2\pi\xi^2}{[1+(k\xi)^2]^{3/2}} \quad (1b)$$

where h' is the magnitude of the random inhomogeneous field arising from sample defects, and ξ is the correlation length of h'. In Fig. 3 we show the result of fitting Eq. (1) to the data allowing $h', \xi,$ and α to vary as fitting parameters and find excellent agreement between theory and experiment using the following values: $h' = 46Oe,\ \xi = 60nm,$ and most importantly $\alpha = 0.03$. We refer the reader to ref. [39] for a complete description of the TMS calculation. The measurements on the isolated single nanomagnet (no Al bars) (Fig. 2(f)) exhibited similar precession frequencies over an extended field range, but consistently larger effective damping values for all applied fields (Fig. 3).

It is worthwhile to discuss the discrepancy between the film and nanomagnet damping behavior, in light of previous studies that have found the intrinsic damping parameter of magnetic materials is not affected by nanopatterning [17,18,43]. First, consider the heat generated by the pump pulse in the nanomagnet which can only dissipate into the HfO_2 film and the substrate beneath, whereas the excess thermal energy in the film can spread laterally because the thermal conductivity (W) of Ni is nearly 2 orders of magnitude larger ($W_{Ni} \sim 90, W_{HfO_2} \sim 1\ W/m\cdot K$). Thus, the temperature of the nanomagnet is significantly higher than the film during the measurement, which could explain the increase in α_{eff}. Indeed, the enhanced damping in the nanostructure is consistent with recent reports that have shown the intrinsic damping of

NiFe films increases monotonically with sample temperature [44]. In addition, we have observed evidence of thermally-assisted oxide formation on the nanomagnet surface when illuminated by the intense pump pulse, which could also contribute to the enhanced damping observed here [45,46].

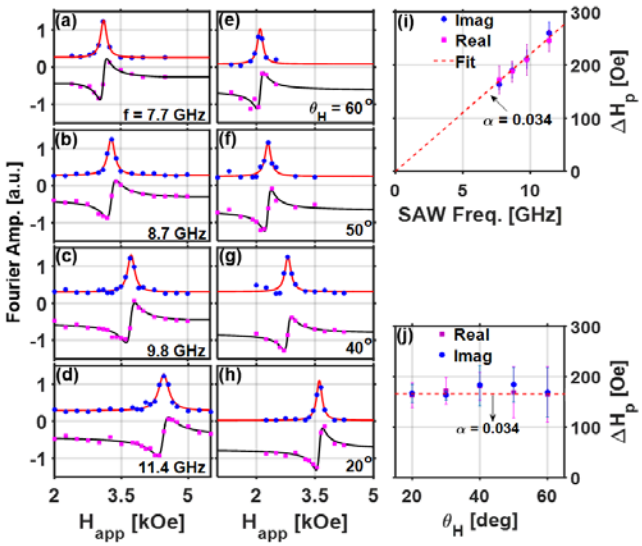

FIG. 4 (color online). Field dependence of the normalized complex Fourier spectra (imaginary Fourier component – circles, real Fourier component – squares) of the MEL driven dynamics at (a)-(d) four distinct SAW frequencies, and (e)-(h) four distinct applied field geometries using a single sample (pitch = 400 nm). (i) Pinning width determined by fitting both the real and imaginary Fourier spectra from Figs. 4(a-d) plotted against f_{SAW} including the fit to Eq. (3) (red dashed line) used to estimate the damping, and (j) summary of ΔH_p from Figs. 4(a),(e)-(h) plotted against θ_H. The data exhibits no significant variation of the pinning width as a function of the applied field angle, which supports the interpretation that the relationship between α and ΔH_p for the nanomagnet is not complicated by extrinsic mechanisms.

Cold excitation at the SAW resonance frequency, however, produces a completely different result. Fig. 2(g) shows that the spin dynamics are strongly excited over a range of fields centered on the resonance field (H_{res}). We again take the DFT of the SAW driven dynamics at each applied field, but now consider the complex Fourier amplitude at the excitation frequency f_{SAW}. The field dependence of the normalized real and imaginary parts of the DFT can be fitted using the following Lorentzian functions [24]:

$$\mathrm{Im}\{F(m_z(t))\} = \frac{1}{2\pi}\frac{\Delta H_p}{(H_{app}-H_{res})^2 + \Delta H_p^2/2} \tag{2}$$

$$\mathrm{Re}\{F(m_z(t))\} = \frac{1}{\pi}\frac{16\Delta H_p (H_{app}-H_{res})}{[4(H_{app}-H_{res})^2 + \Delta H_p^2]^2} \tag{3}$$

to determine H_{res} of the magneto-elastically driven magnetization dynamics as well as the pinning width (ΔH_p). The latter is directly related to the damping and SAW frequency via the relation [24]:

$$\Delta H_p = \alpha_{eff}(H_{app})\frac{4\pi}{\gamma} f_{SAW} \tag{4}$$

We reiterate that for conventional TR-MOKE, the extracted α_{eff} is field-dependent and only converges to the Gilbert damping at high fields [24,38]. For the case of cold excitation, however, the slope of the pinning width as a function of frequency can be used to directly evaluate α. We measured the field-dependent dynamics of four nominally identical Ni nanomagnets, each surrounded by Al bars with different pitch to produce a distinct f_{SAW}. The field-dependence of the complex Fourier spectra taken for each sample were fit using Eqs. (2) and (3) to extract ΔH_p at each SAW frequency (Figs. 4(a)-(d)). Now, the pinning widths display a linear dependence on the resonance frequency as seen in Fig. 4(i). Per Eq. (4), this implies a single damping value for all applied fields. Indeed, we extract a damping value of 0.034, which is nearly identical to the intrinsic damping value determined from the fit to the unpatterned film data using Eq. (1). The damping extracted from the pinning width of the Ni nanomagnet does not depend on the applied field, unlike the conventional TR-MOKE measurements as shown in Fig. 3. This suggests that this technique can be used to directly determine the intrinsic Gilbert damping of nanostructures from a single resonance, unobscured by extrinsic contributions which we will briefly discuss.

First, we note the absence of the y-intercept parameter commonly included in Eq. (4) that is ascribed to inhomogeneous broadening of the resonance. This omission is justified by the fact that the spin wave is necessarily homogenous for a single eigen-mode, as previous studies on similar nanomagnets have reported [17,43,47,48]. Furthermore, we observe no evidence of TMS based on the pinning width analysis of the MEL driven nanomagnet. This can be understood by considering the set of discrete wave vectors in the nanomagnet determined via the relation $k = n\pi/L$, where L is the relevant lateral dimension and n is an odd integer as discussed in refs [49,50]. It is well known [51,52] that the spin wave frequencies increase monotonically for all $\boldsymbol{k}$ that satisfy $\frac{2A_{ex}k^2}{M_s} >> 1$, where $A_{ex} \sim 6x10^7$ *erg/cm* is the exchange constant of Ni. For the 200 nm nanomagnet here, we calculate $\frac{2A_{ex}k^2}{M_s} \approx 100n^2$, which suggests TMS is not operative because there are no degenerate spin waves to facilitate scattering [53,54]. Lastly, we consider the extrinsic contribution to the damping arising from intralayer spin-pumping between the

center and edge modes in the nanomagnet [18]. Based on the single mode behavior shown in Fig. 2(f), we conclude that this mechanism is likely inconsequential here [37].

To further support the conjecture that this method provides a direct measurement of α, we now discuss the MEL driven dynamics measured at various θ_H for the sample with Al bars on a pitch of 400 nm. The results are summarized in Fig. 4(j) and show nearly identical ΔH_p and α values for all θ_H, which is again consistent with the notion that there are no significant extrinsic contributions to the damping. These findings are in stark contrast with ref. [24] which found that α_{eff} decreased monotonically with increasing SAW frequency (or increasing H_{app}). However, in that study the initial conditions were vastly different because the nanomagnets being probed were also the source of the SAWs, thus the magnetic and acoustic oscillations were simultaneously excited by rapid thermalization. Hence, the advantages of our non-local, magneto-elastic approach are clear. This technique provides the single nanomagnet sensitivity of established TR-MOKE detection and well-defined, resonant excitation of the spin dynamics without heating the magnetic system, thereby yielding a direct measurement of the Gilbert damping parameter.

In conclusion, we have demonstrated a novel technique that utilizes non-locally generated SAWs to drive narrowband "cold" excitation of the magnetization precession in a remote single nanomagnet. Using this method, we report the first time-resolved measurements of MEL driven magnetization dynamics of a single Ni nanomagnet. We showed that the intrinsic Gilbert damping can be directly extracted from the applied field range over which magnetic precessions are excited. This finding is in stark contrast from optically excited precessions of single nanomagnets which show larger effective damping that is likely due to the thermal character. In addition to providing a new method to probe transient magnetic behavior in nanostructured materials, elastically driven spin dynamics may be used to improve the switching behavior of magnetic elements for low-energy data storage and memory devices.

We acknowledge T. Yuzvinsky and the W.M. Keck Center for Nanoscale Optofluidics at UC Santa Cruz. This work was supported by the National Science Foundation under Grants No. ECCS-1509020 and DMR-1506104 and the SGMI program by Samsung Inc.

[1] B. Behin-Aein, D. Datta, S. Salahuddin, and S. Datta, Nat. Nanotechnol. **5**, 266 (2010).

[2] J. Torrejon, M. Riou, F. A. Araujo, S. Tsunegi, G. Khalsa, D. Querlioz, P. Bortolotti, V. Cros, K. Yakushiji, A. Fukushima, H. Kubota, S. Yuasa, M. D. Stiles, and J. Grollier, Nature **547**, 428 (2017).

[3] J. Z. Sun, Phys. Rev. B **62**, 570 (2000).

[4] B. Rana, D. Kumar, S. Barman, S. Pal, Y. Fukuma, Y. Otani, and A. Barman, ACS Nano **5**, 9559 (2011).

[5] A. Barman and S. Barman, Phys. Rev. B **79**, 144415 (2009).

[6] H. T. Nembach, J. M. Shaw, T. J. Silva, W. L. Johnson, S. A. Kim, R. D. McMichael, and P. Kabos, Phys. Rev. B **83**, 094427 (2011).

[7] H. J. Chia, F. Guo, L. M. Belova, and R. D. McMichael, Phys. Rev. Lett. **108**, 087206 (2012).

[8] M. Y. Im, P. Fischer, K. Yamada, T. Sato, S. Kasai, Y. Nakatani, and T. Ono, Nat. Commun. **3**, 983 (2012).

[9] O. Klein, G. de Loubens, V. V. Naletov, F. Boust, T. Guillet, H. Hurdequint, A. Leksikov, A. N. Slavin, V. S. Tiberkevich, and N. Vukadinovic, Phys. Rev. B **78**, 144410 (2008).

[10] T. Mewes, J. Kim, D. V. Pelekhov, G. N. Kakazei, P. E. Wigen, S. Batra, and P. C. Hammel, Phys. Rev. B **74**, 144424 (2006).

[11] K. Perzlmaier, M. Buess, C. H. Back, V. E. Demidov, B. Hillebrands, and S. O. Demokritov, Phys. Rev. Lett. **94**, 057202 (2005).

[12] T. Sebastian, Y. Kawada, B. Obry, T. Brächer, P. Pirro, D. A. Bozhko, A. A. Serga, H. Naganuma, M. Oogane, Y. Ando, and B. Hillebrands, J. Phys. D. Appl. Phys. **48**, 164015 (2015).

[13] K. Vogt, H. Schultheiss, S. J. Hermsdoerfer, P. Pirro, A. A. Serga, and B. Hillebrands, Appl. Phys. Lett. **95**, 182508 (2009).

[14] S. Wintz, V. Tiberkevich, M. Weigand, J. Raabe, J. Lindner, A. Erbe, A. Slavin, and J. Fassbender, Nat. Nanotechnol. **11**, 948 (2016).

[15] S. Zhang, S. A. Oliver, N. E. Israeloff, and C. Vittoria, Appl. Phys. Lett. **70**, 2756 (1997).

[16] A. Barman, S. Wang, J. D. Maas, A. R. Hawkins, S. Kwon, A. Liddle, J. Bokor, and H. Schmidt, Nano Lett. **6**, 2939 (2006).

[17] G. D. Fuchs, J. C. Sankey, V. S. Pribiag, L. Qian, P. M. Braganca, A. G. F. Garcia, E. M.

Ryan, Z. P. Li, O. Ozatay, D. C. Ralph, and R. A. Buhrman, Appl. Phys. Lett. **91**, 062507 (2007).

[18] H. T. Nembach, J. M. Shaw, C. T. Boone, and T. J. Silva, Phys. Rev. Lett. **110**, 117201 (2013).

[19] M. Foerster, F. Macià, N. Statuto, S. Finizio, A. Hernández-Mínguez, S. Lendínez, P. V. Santos, J. Fontcuberta, J. M. Hernàndez, M. Kläui, and L. Aballe, Nat. Commun. **8**, 407 (2017).

[20] J. V. Jäger, A. V. Scherbakov, B. A. Glavin, A. S. Salasyuk, R. P. Campion, A. W. Rushforth, D. R. Yakovlev, A. V. Akimov, and M. Bayer, Phys. Rev. B **92**, 020404(R) (2015).

[21] M. Weiler, H. Huebl, F. S. Goerg, F. D. Czeschka, R. Gross, and S. T. B. Goennenwein, Phys. Rev. Lett. **108**, 176601 (2012).

[22] Y. Yahagi, B. Harteneck, S. Cabrini, and H. Schmidt, Phys. Rev. B **90**, 140405(R) (2014).

[23] Y. Yahagi, C. R. Berk, B. D. Harteneck, S. D. Cabrini, and H. Schmidt, Appl. Phys. Lett. **104**, 162406 (2014).

[24] Y. Yahagi, C. Berk, B. Hebler, S. Dhuey, S. Cabrini, M. Albrecht, and H. Schmidt, J. Phys. D. Appl. Phys. **50**, 17LT01 (2017).

[25] S. Wang, A. Barman, H. Schmidt, J. D. Maas, A. R. Hawkins, S. Kwon, B. Harteneck, S. Cabrini, and J. Bokor, Appl. Phys. Lett. **90**, 252504 (2007).

[26] N. Qureshi, H. Schmidt, and A. R. Hawkins, Appl. Phys. Lett. **85**, 431 (2004).

[27] N. Qureshi, S. Wang, M. A. Lowther, A. R. Hawkins, S. Kwon, A. Liddle, J. Bokor, and H. Schmidt, Nano Lett. **5**, 1413 (2005).

[28] V. Sampath, N. D'Souza, D. Bhattacharya, G. M. Atkinson, S. Bandyopadhyay, and J. Atulasimha, Nano Lett. **16**, 5681 (2016).

[29] C. Giannetti, B. Revaz, F. Banfi, M. Montagnese, G. Ferrini, F. Cilento, S. Maccalli, P. Vavassori, G. Oliviero, E. Bontempi, L. E. Depero, V. Metlushko, and F. Parmigiani, Phys. Rev. B **76**, 125413 (2007).

[30] R. Brandt, F. Ganss, R. Rückriem, T. Senn, C. Brombacher, P. Krone, M. Albrecht, and H. Schmidt, Phys. Rev. B **86**, 094426 (2012).

[31] M. Jaris, D. Lau, V. Sokalski, and H. Schmidt, J. Appl. Phys. **121**, 163903 (2017).

[32] B. Koopmans, *Laser-Induced Magnetization Dynamics, in: B. Hillebrands,Spin Dynamics in Confined Magnetic Structures II* (Springer, Berlin, 2003).

[33] B. Koopmans, *Spin Dynamics in Confined Magnetic Structures II* (Springer, Berlin, 2003).

[34] J. Fassbender, *Spin Dynamics in Confined Magnetic Structures II* (Springer, Berlin, 2003).

[35] G. Malinowski, K. C. Kuiper, R. Lavrijsen, H. J. M. Swagten, and B. Koopmans, Appl. Phys. Lett. **94**, 102501 (2009).

[36] Y. Yahagi, B. Harteneck, S. Cabrini, and H. Schmidt, Photonic Phononic Prop. Eng. Nanostructures V **9371**, 93711O (2015).

[37] J. Dubowik, K. Zał□ski, H. Głowiński, and I. Gościańska, Phys. Rev. B **84**, 184438 (2011).

[38] A. Capua, S. Yang, T. Phung, and S. S. P. Parkin, Phys. Rev. B **92**, 224402 (2015).

[39] S. Iihama, A. Sakuma, H. Naganuma, M. Oogane, S. Mizukami, and Y. Ando, Phys. Rev. B **94**, 174425 (2016).

[40] R. Arias and D. L. Mills, Phys. Rev. B **60**, 7395 (1999).

[41] J. Lindner, I. Barsukov, C. Raeder, C. Hassel, O. Posth, R. Meckenstock, P. Landeros, and D. L. Mills, Phys. Rev. B **80**, 224421 (2009).

[42] J. M. Beaujour, D. Ravelosona, I. Tudosa, E. E. Fullerton, and A. D. Kent, Phys. Rev. B **80**, 180415(R) (2009).

[43] S. Tsunegi, H. Kubota, S. Tamaru, K. Yakushiji, M. Konoto, A. Fukushima, T. Taniguchi, H. Arai, H. Imamura, and S. Yuasa, Appl. Phys. Express **7**, 033004 (2014).

[44] Y. Zhao, Q. Song, S. H. Yang, T. Su, W. Yuan, S. S. P. Parkin, J. Shi, and W. Han, Sci. Rep. **6**, 22890 (2016).

[45] L. De Los Santos Valladares, A. Ionescu, S. Holmes, C. H. W. Barnes, A. Bustamante Domínguez, O. Avalos Quispe, J. C. González, S. Milana, M. Barbone, A. C. Ferrari, H. Ramos, and Y. Majima, J. Vac. Sci. Technol. B **32**, 051808 (2014).

[46] J. C. Sankey, P. M. Braganca, A. G. F. Garcia, I. N. Krivorotov, R. A. Buhrman, and D. C. Ralph, Phys. Rev. Lett. **96**, 227601 (2006).

[47] M. L. Schneider, J. M. Shaw, A. B. Kos, T. Gerrits, T. J. Silva, and R. D. McMichael, J. Appl. Phys. **102**, 103909 (2007).

[48] A. Barman, S. Wang, J. Maas, A. R. Hawkins, S. Kwon, J. Bokor, A. Liddle, and H. Schmidt, Appl. Phys. Lett. **90**, 202504 (2007).

[49] S. M. Rezende, F. M. de Aguiar, and A. Azevedo, Phys. Rev. B **73**, 094402 (2006).

[50] C. E. Patton, Phys. Rep. **103**, 251 (1984).

[51] B. A. Kalinikos and A. N. Slavin, J. Phys. C Solid State Phys. **19**, 7013 (1986).

[52] G. Counil, J.-V. Kim, T. Devolder, C. Chappert, K. Shigeto, and Y. Otani, J. Appl. Phys. **95**, 5646 (2004).

[53] J. Jorzick, S. O. Demokritov, B. Hillebrands, B. Bartenlian, C. Chappert, D. Decanini, F. Rousseaux, and E. Cambril, Appl. Phys. Lett. **75**, 3859 (1999).

[54] J. Jorzick, S. O. Demokritov, B. Hillebrands, B. Bartenlian, C. Chappert, D. Decanini, F. Rousseaux, and E. Cambril, J. Appl. Phys. **87**, 5082 (2000).